Asymptotic exponents from low-Reynolds-number flows

Jörg Schumacher[1,4]**, Katepalli R Sreenivasan**[2] **and Victor Yakhot**[3]

[1] Department of Mechanical Engineering, Technische Universität Ilmenau, D-98684 Ilmenau, Germany
[2] International Centre for Theoretical Physics, 34014 Trieste, Italy
[3] Department of Aerospace and Mechanical Engineering, Boston University, Boston, MA 02215, USA
E-mail: joerg.schumacher@tu-ilmenau.de, krs@ictp.it, vy@bu.edu

Abstract. The high-order statistics of fluctuations in velocity gradients in the crossover range from the inertial to the Kolmogorov and sub-Kolmogorov scales are studied by direct numerical simulations (DNS) of homogeneous isotropic turbulence with vastly improved resolution. The derivative moments for orders $0 \leqslant n \leqslant 8$ are represented well as powers of the Reynolds number, *Re*, in the range $380 \leqslant Re \leqslant 5275$, where *Re* is based on the periodic box length L_x. These *low-Reynolds-number flows* give no hint of scaling in the inertial range even when extended self-similarity is applied. Yet, the DNS scaling exponents of velocity gradients agree well with those deduced, using a recent theory of anomalous scaling, from the scaling exponents of the longitudinal structure functions at *infinitely high Reynolds numbers*. This suggests that the asymptotic state of turbulence is attained for the velocity gradients at far lower Reynolds numbers than those required for the inertial range to appear. We discuss these findings in the light of multifractal formalism. Our numerical studies also resolve the crossover of the velocity gradient statistics from Gaussian to non-Gaussian behaviour that occurs as the Reynolds number is increased.

[4] Author to whom any correspondence should be addressed.

IOP Institute of Physics Φ DEUTSCHE PHYSIKALISCHE GESELLSCHAFT

Contents

1. Introduction

1.1. Motivation and previous work

A deep understanding of the turbulent flow field $\mathbf{u}(\mathbf{x}, t)$ remains a challenging problem. Extensions of the classical theory of turbulence by Kolmogorov [1] consider a multiplicity of algebraic scaling exponents for moments of velocity increments $\delta_r u$ in the inertial range of length scales r, which are spanned roughly between the Kolmogorov dissipation scale η_K and the outer scale of turbulence L. The longitudinal increment moments (or structure functions) are then given as

$$S_n(r) \equiv \overline{(\delta_r u)^n} = \overline{\left((\mathbf{u}(\mathbf{x} + \mathbf{r}) - \mathbf{u}(\mathbf{x}))\cdot\frac{\mathbf{r}}{r}\right)^n} = A_n \left(\frac{r}{L}\right)^{\zeta_n}, \tag{1}$$

where the scaling exponents ζ_n depend nonlinearly on the order n but not on the Reynolds number Re, as long as the latter is sufficiently large. The dimensional coefficients A_n depend at most on large-scale quantities. This nonlinear dependence of the algebraic scaling exponents ζ_n on the moment order n is a manifestation of the inertial-range intermittency, which is generally agreed to be an important feature of three-dimensional turbulence. Inertial-range intermittency was experimentally first quantified by Anselmet *et al* [2]. Starting with the work of Kolmogorov [3] and Oboukhov [4], numerous phenomenological models have been developed to study and describe intermittency (see, for example, [5]). The most dominant underlying theme of these models has been the multifractal formalism (MF) [6].

There is a similar intermittency in the dissipative scales. This, too, has been experimentally characterized since [7], and many models have been developed as well (see, again, [5] for a summary). The relation between the two intermittencies has been the subject of the so-called refined similarity hypothesis (RSH) put forth in [3]. This hypothesis links the statistics of the

velocity increments at inertial scales with that of the velocity gradients at smaller scales where inertial and viscous ranges match.

In [7, 8], it was recognized that dissipation intermittency implies an infinite number of dissipative scales, η. Using this insight, Nelkin [9] worked out the Reynolds number dependence of the moments of velocity derivatives. Frisch and Vergassola [10] denoted the range of dissipation scales spanning between $\eta_{\min}$ and $\eta_{\max}$ as the intermediate dissipation range. Their geometric picture of the continuum of dissipation scales is that each element of the range would possess a local Hölder exponent h, which characterizes the spatial roughness of subsets of velocity increments in the inertial range. Consequently, the minimum and maximum values of the dissipation scale would be controlled by the smallest and the largest Hölder exponents: $\eta_{\min} = \eta(h_{\min})$ and $\eta_{\max} = \eta(h_{\max})$. Later, Chevillard *et al* [11] studied the intermediate dissipation range within a random cascade model that takes $\delta_r u$ as a product of a Gaussian random variable and a positive (scale-dependent) transfer variable. They found that $\ln(\eta_{\max}/\eta_{\min}) \sim \sqrt{\ln Re}$. The relation of the intermediate dissipation range to the decay of energy spectra was discussed recently in the context of well-resolved shell models [12].

Efforts have also been made to obtain $\zeta_n(n)$ directly from the Navier–Stokes equations but the problem has remained a great challenge. We limit ourselves here to citing the work of Yakhot [13]—in part because of the connection to the present work and in part because the author kept his considerations close to the dynamical equations. The theory has been extended [14, 15] to explore the connection between the viscous and inertial range intermittencies. This extension builds on the notion that the fluctuating dissipation scale η is to be considered a field that varies in space and time. A relevant feature of the theory is its prediction for the scaling of velocity gradients in terms of the exponents ζ_n.

Within this overall framework, the present paper accomplishes the following goals. Firstly, we perform direct numerical simulations (DNS) of homogeneous isotropic turbulence with vastly better spectral resolution than any previous study. As was explicitly stated by Nelkin [9], such superfine resolutions are required to compute the derivatives accurately. Secondly, we then study the relation between the inertial and dissipative regions within the framework of existing theories, namely RSH and the theory of [14, 15]. After describing the theoretical basis [14, 15] and the details of the numerical simulations (section 1), we discuss the analyticity and scaling of the velocity increment moments in section 2 and present our findings on the velocity gradient statistics in section 3. We also compare in section 3 our results with those of previous work, study in detail the crossover of the statistics of the velocity gradients from Gaussian to non-Gaussian regime and discuss our results in the light of the MF.

Perhaps the most surprising result of the present work is that, while we find no evidence for the inertial range in the DNS data (even when examined through the extended self-similarity (ESS)), the measured scaling exponents of velocity gradients agree well with those deduced from the longitudinal structure functions at *infinitely high Reynolds numbers*. This suggests that the asymptotic state of turbulence is attained for the velocity gradients at far lower Reynolds numbers, well short of those required for the inertial range to appear. We conclude with a summary and an outlook in section 4.

1.2. Numerical simulations

The Navier–Stokes equations for an incompressible Newtonian fluid $\mathbf{u}(\mathbf{x}, t)$ are solved in a periodic box of side length $L_x = 2\pi$. The pseudospectral method is applied with a 2/3

de-aliasing for the fast Fourier transforms. Advancement in time is done by a second-order predictor–corrector scheme. The equations are given by

$$\frac{\partial \mathbf{u}}{\partial t} + (\mathbf{u} \cdot \nabla)\mathbf{u} = -\nabla p + \nu\Delta\mathbf{u} + \mathbf{f}. \tag{2}$$

The kinematic pressure field is $p(\mathbf{x}, t)$ and ν is the kinematic viscosity. We consider flows that are sustained by a volume-forcing $\mathbf{f}(\mathbf{x}, t)$ in a statistically stationary turbulent state. This driving is implemented in the Fourier space for the modes with the largest wavenumbers k_f only, i.e. $k_f^{-1} \approx L_x$. The kinetic energy is injected at a fixed rate ϵ_{in} into the flow. The volume forcing is established by the expression [16, 17]

$$\mathbf{f}(\mathbf{k}, t) = \epsilon_{in}\frac{\mathbf{u}(\mathbf{k}, t)}{\sum_{\mathbf{k}_f \in K}|\mathbf{u}(\mathbf{k}_f, t)|^2}\delta_{\mathbf{k},\mathbf{k}_f}, \tag{3}$$

where the wavevector subset K contains $\mathbf{k}_f = (1, 1, 2)$ and $(1,2,2)$ plus all permutations with respect to components and signs. This energy injection mechanism prescribes the mean energy dissipation rate; that is, the magnitude of the first moment of the energy dissipation rate field, $\overline{\mathcal{E}}$, is determined by the injection rate, ϵ_{in}, having no Reynolds number dependence. This can be seen as follows. Given the periodic boundary conditions in our system, the turbulent kinetic energy balance, which results from rewriting (2) in the Fourier space, reads as:

$$\frac{\mathrm{d}E_{kin}}{\mathrm{d}t} = -\nu\sum_{\mathbf{k}}k^2|\mathbf{u}(\mathbf{k}, t)|^2 + \sum_{\mathbf{k}}\mathbf{f}(\mathbf{k}, t)\cdot\mathbf{u}^*(\mathbf{k}, t). \tag{4}$$

The first term on the right-hand side of (4) is the volume average of the energy dissipation field. Additional time averaging in combination with (3) results in

$$\nu\sum_{\mathbf{k}}k^2\langle|\mathbf{u}(\mathbf{k}, t)|^2\rangle_t = \overline{\mathcal{E}} = \epsilon_{in} = \sum_{\mathbf{k}}\langle\mathbf{f}(\mathbf{k}, t)\cdot\mathbf{u}^*(\mathbf{k}, t)\rangle_t. \tag{5}$$

The applied driving thus allows full control of the Kolmogorov scale $\eta_K = \nu^{3/4}/\overline{\mathcal{E}}^{1/4}$ in comparison to the grid spacing. In contrast to the usually applied stochastic forcing, the integral length scale L, which is defined [18] as

$$L = \frac{\pi}{2\overline{u_x^2}}\int_0^\infty \mathrm{d}k\frac{E(k)}{k}, \tag{6}$$

decreases with increasing Reynolds number. Since the forcing scale in the computations is proportional to the box size, we use the box size L_x as the relevant scale. The use of the integral scale instead of L_x does not alter the scaling results significantly. Further details on the simulation parameters can be found in table 1.

As already pointed out, the adequate resolution of the analytic part of structure functions turns out to be very demanding. The resolution in the present simulations exceed those of conventional simulations by a factor $O(10)$. Consequently, the Reynolds numbers attained are modest despite the relatively large computational box, very much in the spirit of [19]. In order to stress this point further, we compare the statistics of the energy dissipation field $\mathcal{E}(\mathbf{x}, t) = \frac{\nu}{2}(\partial u_i/\partial x_j + \partial u_j/\partial x_i)^2$ for our resolution and the standard case (see figure 1). At least for the intended analysis of higher-order gradient statistics, proper resolution of the far tails turns out to be necessary.

Table 1. Parameters of the DNS. Here, ν is the kinematic viscosity, $\overline{\mathcal{E}}$ is the mean energy dissipation rate, $R_\lambda = \sqrt{5/(3\overline{\mathcal{E}}\nu)}u_{\mathrm{rms}}^2$ is the Taylor-microscale Reynolds number. We will use the following definition for the large scale Reynolds number: $Re = u_{\mathrm{rms}}L_x/\nu$ where the box size $L_x = 2\pi$ is taken. $u_{\mathrm{rms}} = (\overline{u_x^2} + \overline{u_y^2} + \overline{u_z^2})^{1/2}$ is used instead of $(\delta_L u)_{\mathrm{rms}}$. The spectral resolution is indicated by $k_{\max}\eta_{\mathrm{K}}$ where $k_{\max} = \frac{\sqrt{2}N}{3}$ and N the number of grid points in each direction of the cube.

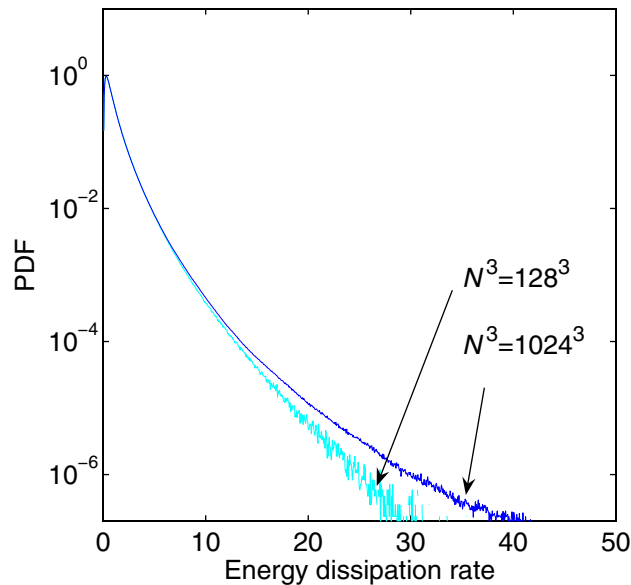| Run no.	N	ν	$\overline{\mathcal{E}}$	u_{rms}	L	R_λ	Re	$k_{\max}\eta_{\mathrm{K}}$
1	512	1/30	0.1	0.687	1.018	10	129	33.56
2	1024	1/75	0.1	0.808	0.920	24	380	33.56
3	1024	1/200	0.1	0.854	0.758	42	1074	15.93
4	1024	1/400	0.1	0.892	0.694	65	2243	9.6
5	2048	1/400	0.1	0.882	0.690	64	2218	19.2
6	2048	1/1000	0.1	0.911	0.659	107	5725	9.6

Figure 1. Resolution requirements in the numerical simulations. The probability density function (PDF) of the energy dissipation field $\mathcal{E}(\mathbf{x}, t) = \nu/2(\partial u_i/\partial x_j + \partial u_j/\partial x_i)^2$ is plotted. The dissipation field is given in units of the mean energy dissipation rate $\overline{\mathcal{E}}$. The case with $k_{\max}\eta_{\mathrm{K}} = 1.2$ (cyan curve), corresponding roughly to the standard resolution in a box of size $N = 128$, is compared with that of superfine resolution (blue curve, see also table 1). While the cores of both PDFs agree, deviations are manifest in the far tails. Both runs are for $R_\lambda = 65$. Approximately 1.7×10^8 data points were processed for the analysis in the low-resolution run; the corresponding number for the high-resolution run was about 30 times larger.

1.3. Theoretical basis

The theory [14, 15] starts with the exact equations for the nth order longitudinal structure functions $S_n(r)$ which can be directly derived from the equations of motion for the turbulent fluid [13, 20]. For homogeneous, isotropic and statistically stationary turbulence in three dimensions these equations take the form

$$\frac{\partial S_{2n}(r)}{\partial r} + \frac{2}{r}S_{2n}(r) = \frac{2(2n-1)}{r}G_{2n-2,2}(r) + (2n-1)\overline{\delta_r a(\delta_r u)^{2n-2}}. \tag{7}$$

Here, $G_{2n-2,2}$ is the mixed term containing longitudinal increments of order $2n-2$ and transverse increments of order 2. Equation (7) is not closed because the last term on the right-hand side is unknown. For small increment scales around the Kolmogorov length, it follows that the expression for the Lagrangian acceleration of fluid particles is given by

$$\delta_\eta a = \frac{(\delta_\eta u)^3}{\nu}, \tag{8}$$

recalling that the characteristic time is of the order $\nu/(\delta_\eta u)^2$. In this equation, note that η is a field and that increments are therefore taken across variable distances. The unknown term has the form

$$\overline{\delta_r a(\delta_r u)^{2n-2}} \approx \frac{1}{\nu}\overline{(\delta_\eta u)^3(\delta_r u)^{2n-2}}. \tag{9}$$

This correlation involves two scales—a locally varying dissipation scale field η in the acceleration increment and r in the velocity increment moment—and is therefore hard to manipulate. However, in the limit $r \to \eta$ one can make some progress. In this limit, we set $\eta = \eta_{2n}$, where η_{2n} is the *order-dependent* matching distance between the analytic and singular parts of $S_{2n}(r)$ (see figure 2). The other three terms of (7) are found to be of the same magnitude [21, 22] and are of the order S_{2n}/η_{2n}. One thus obtains, for $r \to \eta$, the result

$$\frac{S_{2n}(\eta_{2n})}{\eta_{2n}} \approx \frac{S_{2n+1}(\eta_{2n})}{\nu}. \tag{10}$$

Now, the velocity increments have the property that, at the large scale L, their distribution is Gaussian. It then follows from (1) that $S_{2n}(\eta_{2n}) = (2n-1)!!\sigma_L^{2n}(\eta_{2n}/L)^{\zeta_{2n}}$, where $\sigma_L = \sqrt{\overline{(\delta_L u)^2}}$.[4] Putting $r = \eta_{2n}$, one obtains from (5)

$$\left(\frac{\eta_{2n}}{L}\right)^{\zeta_{2n}-\zeta_{2n+1}-1} = \frac{(2n)!!}{(2n-1)!!}\frac{\sigma_L L}{\nu} \approx \frac{\sigma_L L}{\nu}. \tag{11}$$

With the large scale Reynolds number $Re = \sigma_L L/\nu$ one gets

$$\eta_{2n} \approx LRe^{\frac{1}{\zeta_{2n}-\zeta_{2n+1}-1}}. \tag{12}$$

For the Kolmogorov scaling, $\zeta_n = \frac{n}{3}$ and (12) yields $\eta_{2n} = LRe^{-3/4} = \eta_K$ for all orders n, as consistency would require.

---

[4] For example, $S_4(L) = 3!!\sigma_L^4(L/L)^{\zeta_4} = 3\sigma_L^4$ and $S_2(L) = \sigma_L^2$. It follows that, at the appropriate large scale L, the flatness factor $S_4(L)/S_2^2(L) = 3$.
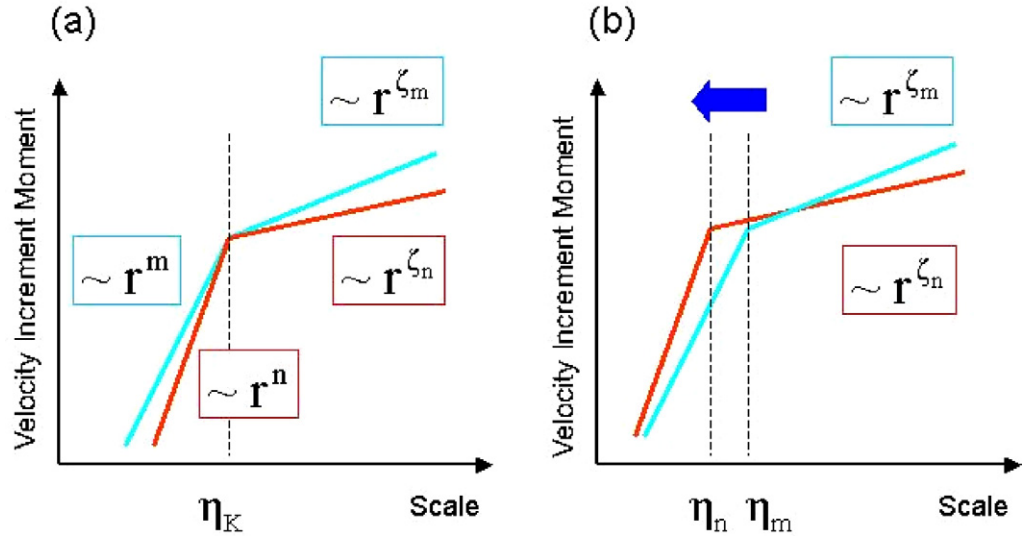
Figure 2. The matching of the inertial and dissipative ranges. (a) In the standard approach, the same Kolomogorov scale matches the singular ($\sim r^{\zeta_n}$) and analytic parts ($\sim r^n$) for all orders n of the increment moments. (b) In the theory of [14, 15], for each order of the moment $S_n(r)$, the singular and analytic parts match at an order-dependent scale η_n. Following (12), $\eta_n < \eta_m$ when $n > m$.

To make further progress, the functional dependence of ζ_{2n} has to be given explicitly. The theory of [13] provides a convenient functional form

$$\zeta_{2n} = \frac{2(1+3\beta)n}{3(1+2\beta n)},\tag{13}$$

which, with the free fitting parameter β set to 0.05, agrees with available experimental data in high-Reynolds-number flows (for order 10–15). We find that this relation agrees, up to order 10–15, with available measurements as well as with popular parametrizations of ζ_n, e.g. with the She–Leveque model and the p-model [23, 24]. The scaling behaviour of the spatial derivative in the analytic range of the displacement r can be calculated, in the limit $r \to \eta$, as

$$\overline{\left|\frac{\partial u}{\partial x}\right|^n} \approx \overline{\left|\frac{\delta_\eta u}{\eta}\right|^n} = \frac{\overline{(\delta_\eta u)^{2n}}}{\nu^n} \propto Re^n \eta_{2n}^{\zeta_{2n}} = Re^{\rho_n},\tag{14}$$

where we have used the fact that the 'dynamic' Reynolds number at the local dissipation scale is unity, i.e. $Re_\eta = \eta \delta_\eta u / \nu \approx 1$. The use of (12) yields

$$\rho_n = n + \frac{\zeta_{2n}}{\zeta_{2n} - \zeta_{2n+1} - 1}.\tag{15}$$

Since $\zeta_3 = 1$ [25], relation (15) gives $\zeta_2 = (2 - 2\rho_1)/(2 - \rho_1)$. For the Kolmogorov value of $\zeta_2 = 2/3$, we obtain $\rho_1 = 1/2$. The anomaly that may exist in the first-order exponent ρ_1 for velocity gradients is related to the second-order inertial exponent ζ_2. For moments of the

IOP Institute of Physics **Φ** DEUTSCHE PHYSIKALISCHE GESELLSCHAFT

dissipation rate, one can write

$$\overline{\mathcal{E}^n} \equiv \nu^n \overline{\left(\frac{\partial u_i}{\partial x_j}\right)^{2n}} \approx \nu^n \overline{\left(\frac{(\delta_\eta u)^2}{\nu}\right)^{2n}} = \frac{\overline{(\delta_\eta u)^{4n}}}{\nu^n} \propto Re^{d_n}, \tag{16}$$

where

$$d_n = n + \frac{\zeta_{4n}}{\zeta_{4n} - \zeta_{4n+1} - 1}. \tag{17}$$

Thus, the second-order quantities for the dissipation rate are expressed in terms of the eighth-order quantities involving velocity increments. In general, to accurately evaluate $\overline{\mathcal{E}^n}$, one has to resolve the analytic range within which $S_{4n}(r) \propto r^{4n}$. This difficulty for large n is one of the main considerations of the theory.

Finally, we note that

$$d_1 = 0 \tag{18}$$

because $\overline{\mathcal{E}} = \epsilon_{\text{in}}$ holds in the DNS (see equation (5)). From relation (17) one immediately has

$$\zeta_5 = 2\zeta_4 - 1. \tag{19}$$

Measurements are, in fact, in good conformity with this equation.

1.4. Velocity gradients from RSH

The RSH [3] imposes a different constraint between moment orders of the energy dissipation and structure functions. This results in a different Reynolds number dependence compared to (17). When taking $\mathcal{E} \sim (\delta_{\eta_K} u)^3 / \eta_K$ the relation

$$\overline{\mathcal{E}^n} \sim \frac{S_{3n}(\eta_K)}{\eta_K^n} \sim \eta_K^{\zeta_{3n} - n}, \tag{20}$$

follows. With $\eta_K = L Re^{-3/4}$ we get

$$\overline{\mathcal{E}^n} \sim Re^{3(n - \zeta_{3n})/4}. \tag{21}$$

The comparison with the present data will be made later in this text (see table 2). Here, we briefly mention that the intermittency exponent μ in the scaling $\overline{\mathcal{E}(\mathbf{x} + \mathbf{r})\mathcal{E}(\mathbf{x})} \sim r^{-\mu}$ is 0.25 from RSH while the application of the theory of [14, 15] gives $\mu \approx 0.2$. Both are within the accepted range of 0.25 ± 0.05.

1.5. Velocity gradients from the MF

Nelkin [9] predicted a Reynolds number dependence for derivative moments based on the MF. The derivation of his expressions relied on the steepest descent approximation of resulting integrals and input from measurements [7]. His result (which is also outlined in detail in [6], pp 157–8) is that

$$\rho_n = p(n) - n, \tag{22}$$

Table 2. Comparison of scaling exponents for different velocity gradient moments. ρ_n for $n = 1, 3, 5, 7$ (see (15)) and d_n (see (17)) for $n = 1, 2, 3, 4$ are listed. Results from the present DNS are compared with those from the theory [14, 15] after inserting (13) into (15) and (17). Comparisons with the RSH and the MF are also provided. The error bars for orders 3 and 4 of the DNS data have been determined from lower and upper envelopes to the tails of $\mathcal{E}^n p(\mathcal{E})$, $p(\mathcal{E})$ being the PDF of the energy dissipation field. The same holds for orders 5 and 7 in the case of $p(|\partial u / \partial x|)$. The range of Reynolds numbers for all fits was 380 to 2243.

	Theory [14]	DNS	RSH	MF
ρ_1	0.465	0.455	–	0.474
ρ_3	1.548	1.478	–	1.573
ρ_4	2.157	2.051	–	2.188
ρ_5	2.806	2.664 ± 0.137	–	2.841
ρ_7	4.203	3.992 ± 0.653	–	4.241
d_1	0.000	0.000	0.000	–
d_2	0.157	0.152	0.173	–
d_3	0.489	0.476 ± 0.009	0.465	–
d_4	0.944	0.978 ± 0.034	0.844	–

in terms of the notation used above. Here $p(n)$ is a unique solution that follows from the intersection of the concave curve ζ_p with the straight line $2n - p$ for a given n. With (13) the intersection ($p > 0$) obeys the relation

$$p(n) \approx -\frac{4 + 3\beta(1 - 2n)}{6\beta} + \frac{1}{6\beta}\sqrt{72\beta n + (3\beta(2n - 1) - 4)^2}. \tag{23}$$

The resulting values of ρ_n are also listed in table 2.

2. Moments of velocity increments

2.1. Rescaling of higher order moments and test of analyticity

Figures 3(a) and (b) show the structure functions $S_{2n}(r)/v_K^{2n}$ plotted against r/η_K for three Reynolds numbers for order 2 ($n = 1$) and 10 ($n = 5$). Here, v_K is the Kolmogorov velocity corresponding to the definition $\eta_K v_K / \nu = 1$. Two features of the graphs are worth noting. Firstly, no inertial range can be seen at these low Reynolds numbers. Secondly, all data possess analytic parts thus confirming that the resolution used is adequate. It is important to recognize in figure 4 that with increase of both the Reynolds number and moment order the width of the analytic range decreases. To make this point more explicit, we plot in figure 4 the compensated structure functions S_{2n}/r^{2n} ($n = 1$–5) for a fixed Reynolds number $R_\lambda = 64$ (left panel) and the normalized moment S_{10}/r^{10} for different Reynolds numbers (right panel). In the analytic range we expect

$$\frac{S_{2n}(r)}{r^{2n}} \to \overline{\left(\frac{\partial u}{\partial x}\right)^{2n}} = \text{constant}, \tag{24}$$
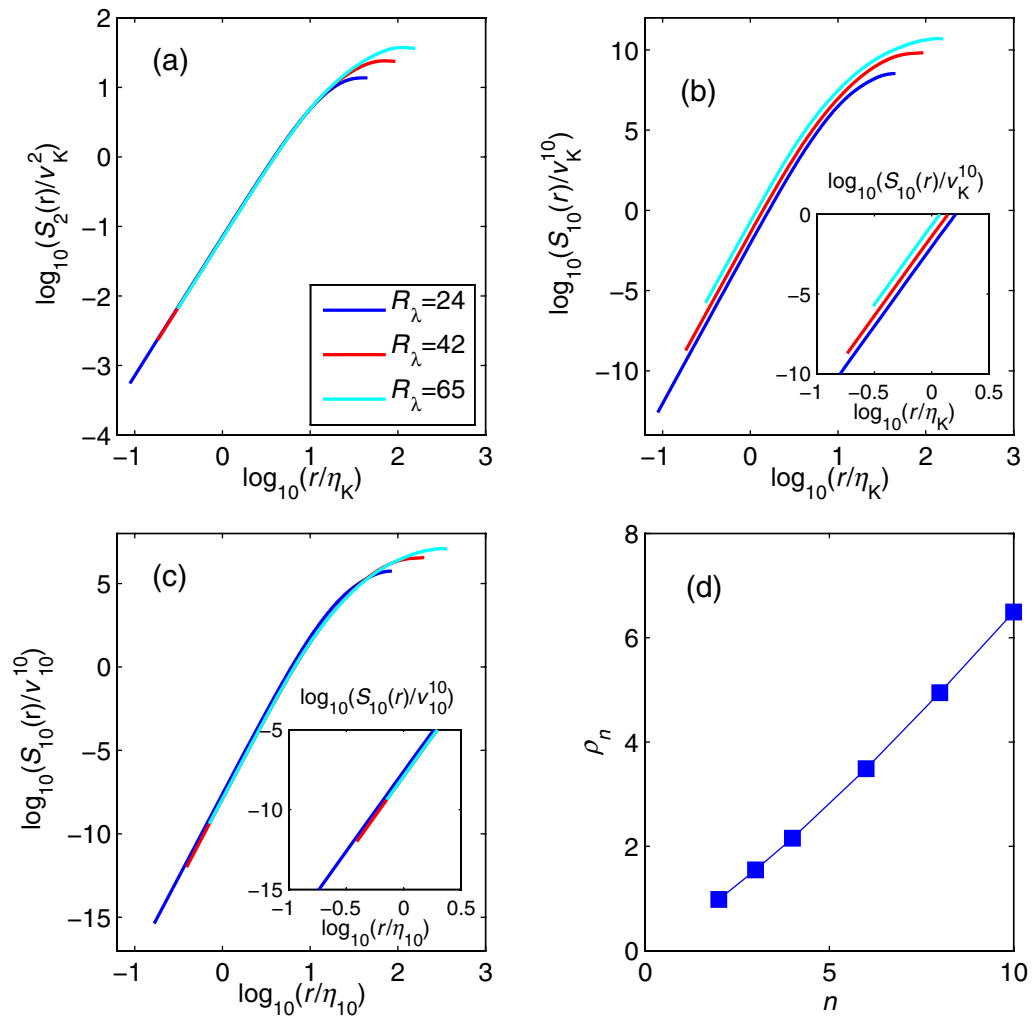
Figure 3. Longitudinal structure functions of the turbulent velocity field. (a) Second-order longitudinal structure function $S_2(r)/v_K^2$ over r/η_K for the three different runs indicated in the legend. (b) Tenth-order longitudinal structure functions $S_{10}(r)/v_K^{10}$ over r/η_K for the same data. The inset shows that the curves do not collapse well. Here, $v_K = (v\bar{\mathcal{E}})^{1/4}$ is the Kolmogorov velocity. (c) The tenth-order structure functions for $R_\lambda = 24, 42, 65$ collapse when r is rescaled by the dissipation scale η_{10} defined by (12) and the amplitudes by the velocity scale v_{10}^{10} (see equation (25)). The inset shows the same level of expansion as in (b). (d) The figure shows the exponent ρ_n as a function of order n given by equations (13) and (15).

i.e. independent of the increment distance r. For $R_\lambda = 64$, this range is well defined for the moments $n \leqslant 3$ and just survives for $n = 5$. This means that, even for the present super-resolution, the representation of moments of velocity derivatives in terms of the low-order finite differences may be problematic for moment orders higher than 5 (although we present data for n up to 8).

In the analytic range, all curves can be expected to collapse when normalized by the appropriate length and velocity scales. The traditional scales are the Kolmogorov length and
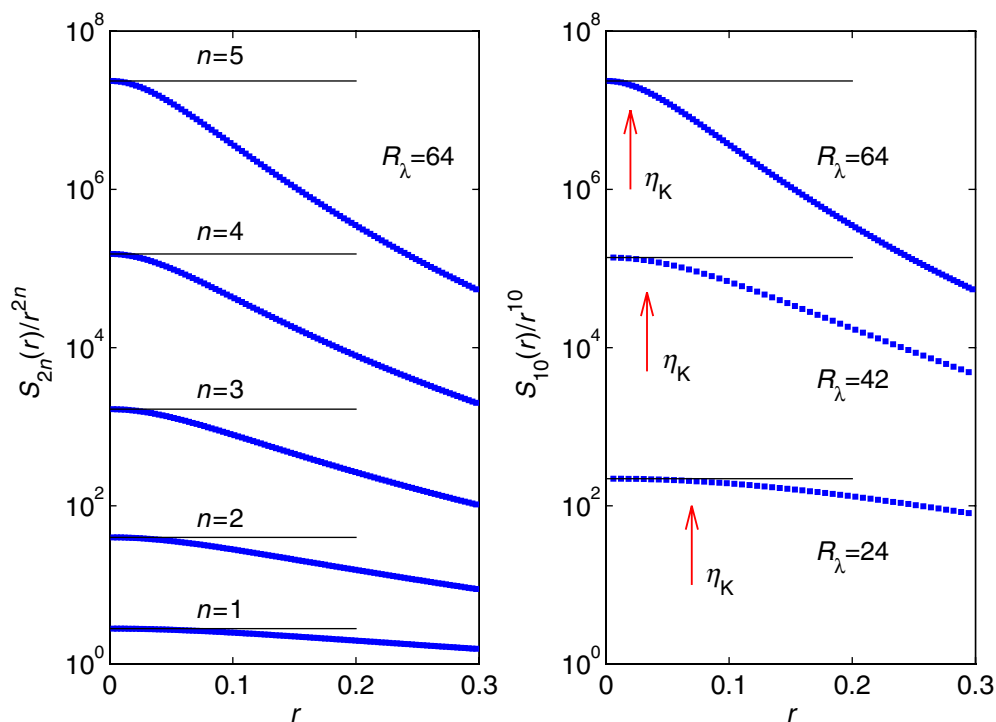
Figure 4. Test of analyticity for the longitudinal structure functions $S_{2n}(r)$ by compensated plots. Left panel: orders $2n = 2, 4, 6, 8, 10$ are shown for run 5. Horizontal lines indicate the exact analytical form corresponding to $S_{2n}(r) \sim r^{2n}$. Right panel: $S_{10}(r)$ is shown for runs 2, 3 and 5. The red vertical arrows indicate the corresponding Kolmogorov scales η_K.

velocity scales η_K and v_K, respectively. This scaling works well for low order moments (say 2), as seen in figure 3(a). The same normalization is not adequate for high orders such as 10, as can be seen in figure 3(b). However, all curves do collapse when the length scale η_{2n} (see equation (12)) and the corresponding velocity scale

$$v_{2n} = \frac{\nu}{\eta_{2n}} \tag{25}$$

are used instead of η_K and v_K (see figure 3(c)).[5]

How can we understand this collapse? Introducing the 'dynamic' Reynolds number $Re_r = r\delta_r u/\nu$, and recalling that the only relevant parameter in the inertial range—including the interval just above the dissipation range ($r \gtrsim \eta$)—is the energy flux, we can conclude that the dynamics of fluctuations at the scales $r \approx \eta$ are independent of the width of the inertial range (L, η). While one cannot, in principle, rule out the existence of other fluxes corresponding to some yet unknown integrals of motion related to structure functions of higher order than 2 [26], this possibility will not influence the essence of the argument. If so, for $r \lesssim \eta$, the properly normalized moment of a given order n must be independent of Re.

---

[5] We note here parenthetically that S_{10} for the lowest Reynolds number ($R_\lambda = 10$) does not collapse on the common curve. For this case, however, the velocity gradient statistics are Gaussian, in contrast to the other three cases. This issue will be discussed in greater detail in section 3.2.
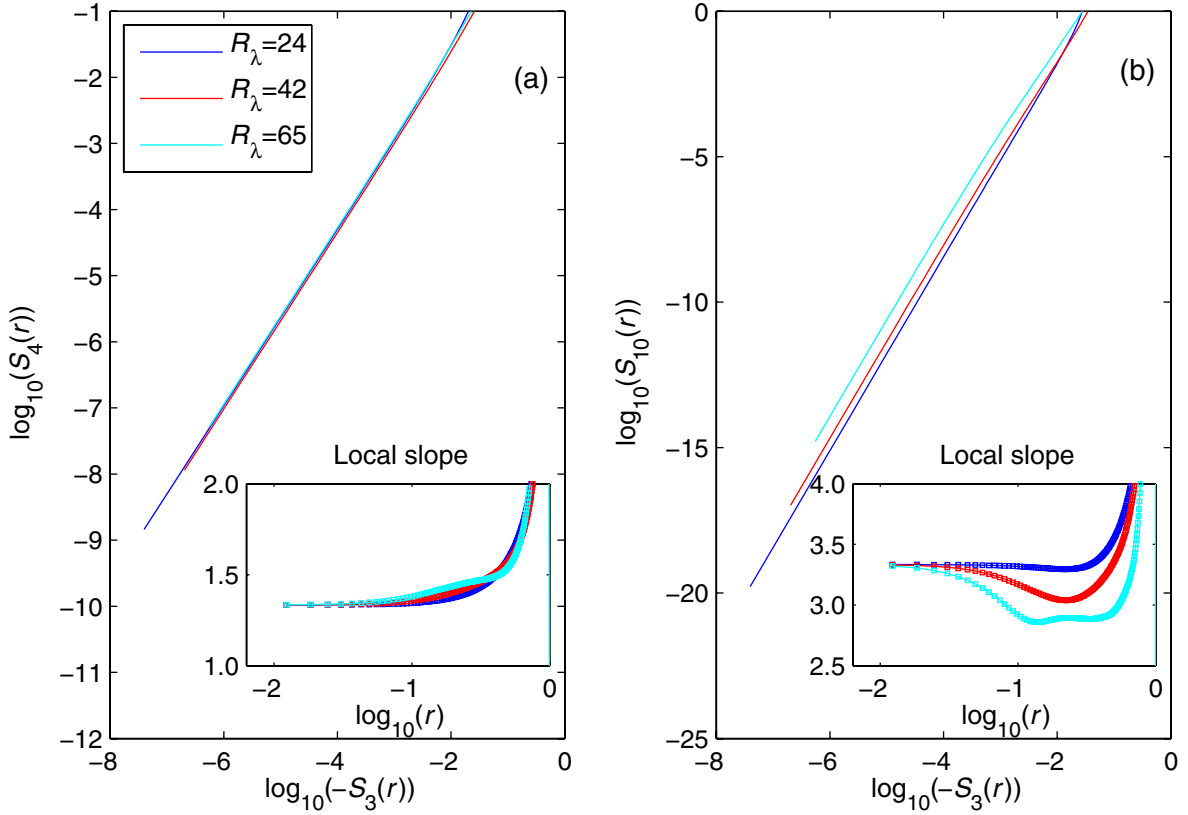
Figure 5. ESS analysis of longitudinal structure functions. (a) Fourth-order structure function $S_4(r)$ versus $-S_3(r)$. Structure functions are defined by equation (1), with $-S_3(r) = (4/5)\overline{\mathcal{E}}r$. (b) Tenth-order structure function $S_{10}(r)$ versus $-S_3(r)$. The insets in both figures show the corresponding local slope $\chi_n(r)$ as given by relation (27). Data for runs 2, 3 and 5 are indicated by different colours, as noted in the legend.

2.2. Test of ESS

Since no inertial-range scaling can be observed for such low Reynolds numbers in the standard double logarithmic plot, we tested the method of ESS by Benzi *et al* [27]. As is well known, the main point of ESS is that even though there is no discernible scaling in the standard plot when the Reynolds numbers are low, one can detect a sizeable range of scaling when arbitrary moment orders are compared with S_3:

$$S_n(r) \sim (-S_3(r))^{\zeta_n}. \tag{26}$$

The sensitive and scale-dependent measure for possible anomalous scaling is then the local slope

$$\chi_n(r) = \frac{\mathrm{d}\ln(S_n(r))}{\mathrm{d}\ln(-S_3(r))}. \tag{27}$$

The results for our data are shown in figure 5 for the fourth- and tenth-order. In both figures we cannot detect anomalous scaling in the ESS framework, which would result in local slopes of

$\chi_4(r) \approx 1.28$ and $\chi_{10}(r) \approx 2.59$ [13, 23]. We conclude that only a further increase of the Reynolds number will shift the local slope towards the asymptotic values. Thus, even the 'backdoor' of ESS is not opened for our small Reynolds numbers. This confirms our statement made before that the velocity field statistics does not have any asymptotic scaling in the inertial range. The inset reveals an interesting feature. It can be observed that a faster relaxation towards anomalous scaling occurs with increasing order. At this point, we can only speculate about the reason for this feature. On one hand, the differences between the viscous scaling, $\chi_n(r) = n/3$, and the inertial scaling, $\chi(r) = \zeta_n$, become larger with increasing order and thus better visible in the local slope. On the other hand, an order-dependence of the dissipation scale, η_n, might cause a slight increase of the inertial range and the crossover between inertial and viscous ranges, respectively.

3. Velocity gradient statistics

3.1. Results and comparison with RSH

If indeed the properties of fluctuations from the interval $r \lesssim \eta$ depend only upon the local magnitude of the energy flux $\overline{\mathcal{E}}$ and not upon the width of the inertial range (L, η), one can hope to obtain the asymptotic values of exponents $\rho_n(Re) \to \rho_n(\infty)$ in reasonably low-Reynolds-number flows, provided that a small (even very small) constant-flux range exists for scales $r > \eta$.

In figure 6, we plot $\overline{|\partial u/\partial x|}$ and $\overline{\mathcal{E}^n}$ as functions of Re. Statistical convergence of both gradient quantities is satisfactory for gradient moments of at least up to the seventh-order (see figure 6(c)) and dissipation moments of at least up to the fourth-order (see figure 6(d)). As can be seen from table 2, the data agree well with theoretical predictions [14, 15]. For example, we get $\rho_1 = 0.455$ compared to the theoretical value of 0.465. The second-order exponent ζ_2 is given by

$$\zeta_2 = \frac{2 - 2\rho_1}{2 - \rho_1} = 0.706, \tag{28}$$

which is very close to the experimental value of $\zeta_2 = 0.71$ [24, 27]. We stress that this result was obtained in flows with $24 \leqslant R_\lambda \leqslant 65$, none of which has any inertial range. The moments of the dissipation rate also agree with theoretical predictions, as shown in table 2.

In the theory outlined earlier [14], the second-, third- and fourth-order moments of $\mathcal{E}$ are related to the structure functions $S_8(\eta_8)$, $S_{12}(\eta_{12})$ and $S_{16}(\eta_{16})$, respectively. These structure functions probe very intense, low-probability velocity fluctuations and, as a result, huge data sets are needed to accurately evaluate their characteristics. We have seen that dissipation moments of order 5 are barely resolved in the present simulations, while the data for the sixth-order moment $\overline{\mathcal{E}^6}$, corresponding to S_{24} have not converged well. In addition, we stress that the statistical convergence is not sufficient for the accurate determination of structure functions: the simulations must resolve accurately at least a fraction of the analytic range $r < \eta_{4n}$.

Table 2 lists comparisons between theoretical considerations and the DNS data. In the case of the dissipation field, we inserted (13) into (21); for the velocity derivative scaling exponents from MF, we used the relation (23) which was inserted into (22). For the gradient exponents, the DNS data are somewhat smaller than both the theory [14, 15] and the multifractal theory.
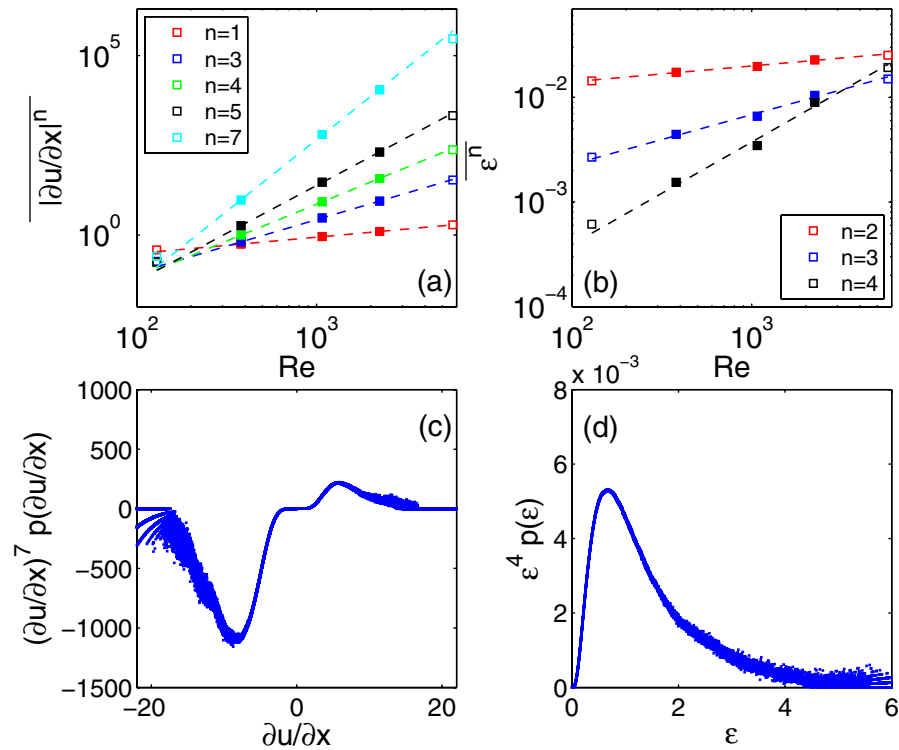
Figure 6. The Reynolds number dependence of the moments of velocity derivative and energy dissipation. (a) Moments of the absolute value of the longitudinal velocity derivative $\partial u/\partial x$ for orders 1, 3, 4, 5 and 7 as functions of the box Reynolds number Re. Only the filled data points were included in the least-square fit, but run 6 demonstrates that the scaling continues for higher Reynolds number. The case with the lowest Reynolds number has Gaussian statistics (as will be described below) and is hence not turbulent in the traditional sense. (b) Moments of order 2, 3 and 4 of the energy dissipation field $\mathcal{E}$. Again, only the filled data points were used for the fit to evaluate the exponent. (c) Statistical convergence test for the seventh-order longitudinal velocity derivative moment at the highest Reynolds number considered here, $R_\lambda = 65$ (run 4). The data set contained 15 samples of the turbulent field which results in 1.6×10^{10} data points. (d) Statistical convergence test of the fourth order moment of the energy dissipation field. Again, data from run 4 are used.

In the case of the dissipation exponents, the DNS results are closer to the theory of [14, 15] and somewhat larger than those of RSH. Note that the results of both theories depend on the inertial scaling exponents obtained from measurements (or at least expressions tuned to agree with measurements). Considering that there are issues of resolution in measurement (although not in the same sense as in simulations), these departures may suggest that inertial exponents may need slight revision. Of course, there might be other reasons for these differences.
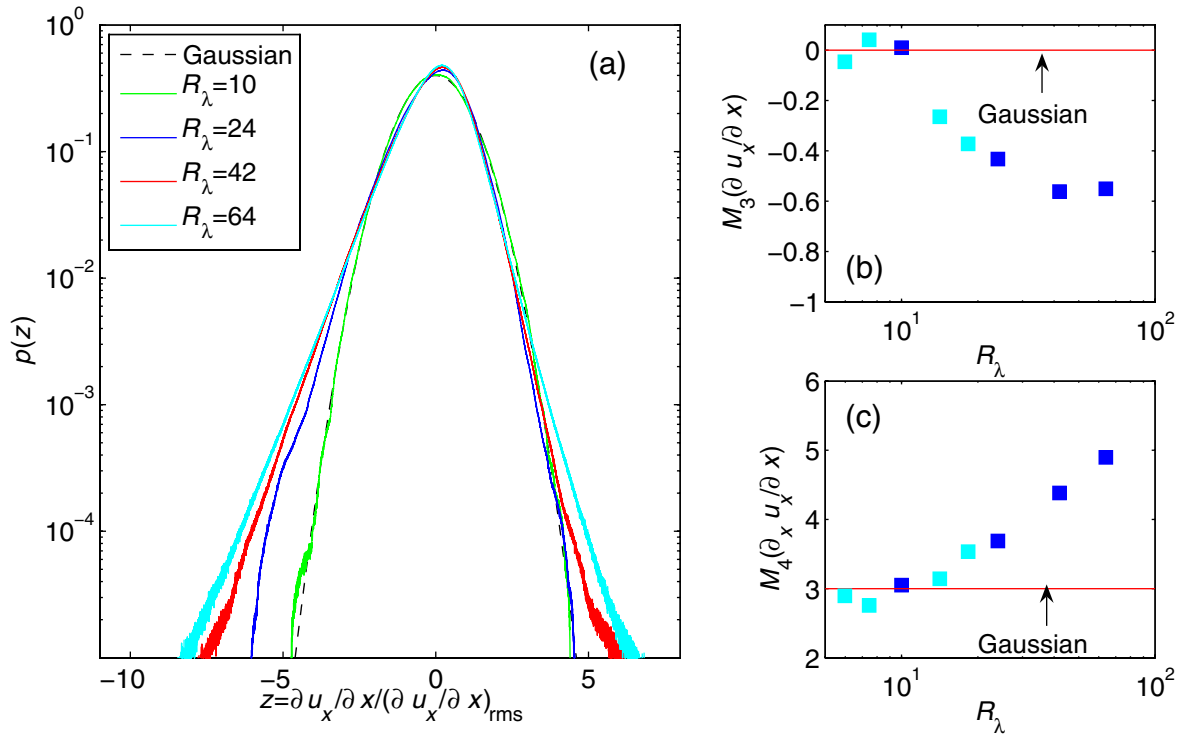
Figure 7. Statistics of the velocity gradient $\partial u / \partial x$. (a) Plots of the PDF for runs 1–4 as indicated in the legend. The gradient is normalized by its root-mean-square value. For comparison the Gaussian distribution is added to the figure. (b) Corresponding skewness of the PDFs (blue symbols). (c) Corresponding flatness of the PDFs (blue symbols). In order to highlight the transition, further data points have been added to the data of table 1 in panels (b) and (c). These additional numerical simulations have been conducted at a spectral resolution of $N = 256$ for different kinematic viscosities. Forcing scheme and energy injection rate are the same as before. The additional data values are plotted as cyan filled squares.

3.2. Transition from Gaussian to non-Gaussian velocity gradient statistics

As mentioned earlier, while computing scaling exponents, run 1 was excluded from the least-square fits. The reason is the qualitatively different nature of the velocity gradient statistics at this lowest Reynolds number ($R_\lambda = 10$). This will be discussed now. Figure 7 illustrates the crossover from Gaussian statistics at very low Reynolds numbers to an increasingly non-Gaussian behaviour for moderate Reynolds numbers. In order to highlight this transition, we generated additional DNS data at intermediate Reynolds numbers. The Gaussian values for the third- and fourth-order normalized derivative moment are indicated by the red solid lines in panels (b) and (c) of figure 7. The derivative moments are defined as

$$M_n(\partial u / \partial x) = \frac{\overline{(\partial u / \partial x)^n}}{\overline{(\partial u / \partial x)^2}^{n/2}}. \tag{29}$$

For the lowest Reynolds numbers we detected a regime which is a complex time-dependent flow rather than a turbulent one. In this regime, the flow can be basically described by the small number of driven modes that form a low-dimensional nonlinear dynamical system. All other degrees of freedom are strongly damped and slaved to the driven modes. The sign of the derivative skewness $M_3(\partial u/\partial x)$ there became sensitively dependent on the particular modes that were driven. Since the non-Gaussian behaviour is related to the acceleration-velocity term in equation (7), the experience suggests that it is difficult to pin down the behaviour of this term near zero. The magnitudes of M_3 and M_4 varied, respectively, around zero and three (even for very long-time runs). We verified this by choosing different wavevectors for driving the flow while leaving all other simulation parameters the same, including the energy injection rate $\epsilon_{\rm in}$ (see equation (5)). At larger Reynolds numbers, $R_\lambda > 10$ or 15, the derivative moments became insensitive to the particular driving. Therefore, our studies suggest that the transition to non-Gaussian statistics is smooth with respect to the Reynolds number and that intermittency continuously grows with the growing number of excited modes.

Figure 8 illustrates the morphological changes of the spatial distribution of the velocity gradient that are connected with the change of the statistical properties. The increasing intermittency of the velocity gradients is accompanied by an increasing fragmentation of the isolevel sets.

4. Summary and discussion

Turbulence in a three-dimensional periodic box, generated by the Navier–Stokes equations driven by a large-scale forcing, was investigated in the Taylor microscale Reynolds numbers range $10 \leqslant R_\lambda \leqslant 107$. The simulations were made at superfine resolution in order to resolve the analytic part of structure functions at least up to order 16. No inertial ranges characterized by the velocity structure functions $S_n(r) \propto r^{\zeta_n}$ were detected—not even with the method of ESS. In the range $24 \leqslant R_\lambda \leqslant 107$, strong intermittency of the spatial derivatives was detected and their moments were accurately described by the scaling relations $\overline{|\partial u/\partial x|^n} \propto Re^{\rho_n}$ and $\overline{\mathcal{E}^n} \propto Re^{d_n}$, respectively. The exponents ρ_n and d_n were found to be essentially in agreement with the theoretical work for high Reynolds number [14, 15]. Based on the well-resolved numerical results, we are thus able to relate the dissipation-range exponents of the velocity gradients to the inertial range scaling exponents of the velocity field for very high Reynolds numbers. For instance, the DNS result $\rho_1 \approx 0.455$ gives $\zeta_2 = 0.706$ corresponding to the asymptotic high-Reynolds number energy spectrum $E(k) \propto k^{-1.706}$.

The competing theoretical predictions are from RSH (for dissipation) and the multifractal theory (for the gradients). They, too, agree with the DNS results, although somewhat less successfully overall. It appears that the theory of [14, 15] seems to have an edge.

This last conclusion would have been more conclusive if we had been able to obtain reliable dissipation range statistics accurately for moments of order 5 or 6. Despite the huge data sets of $\approx 10^{10}$ points, we were unable to obtain reliable data for dissipation field moments with $n > 4$, certainly for n no larger than 5. The theory suggests the reason for this problem: moments of the dissipation rate $\overline{\mathcal{E}^n}$ are related to high-order structure functions $S_{4n}(\eta_{4n})$ probing very low probability fluctuations evaluated on the corresponding dissipation scales.

We also conducted simulations at various Reynolds numbers to study the smooth transition of the velocity gradient statistics from Gaussian behaviour to non-Gaussian behaviour.
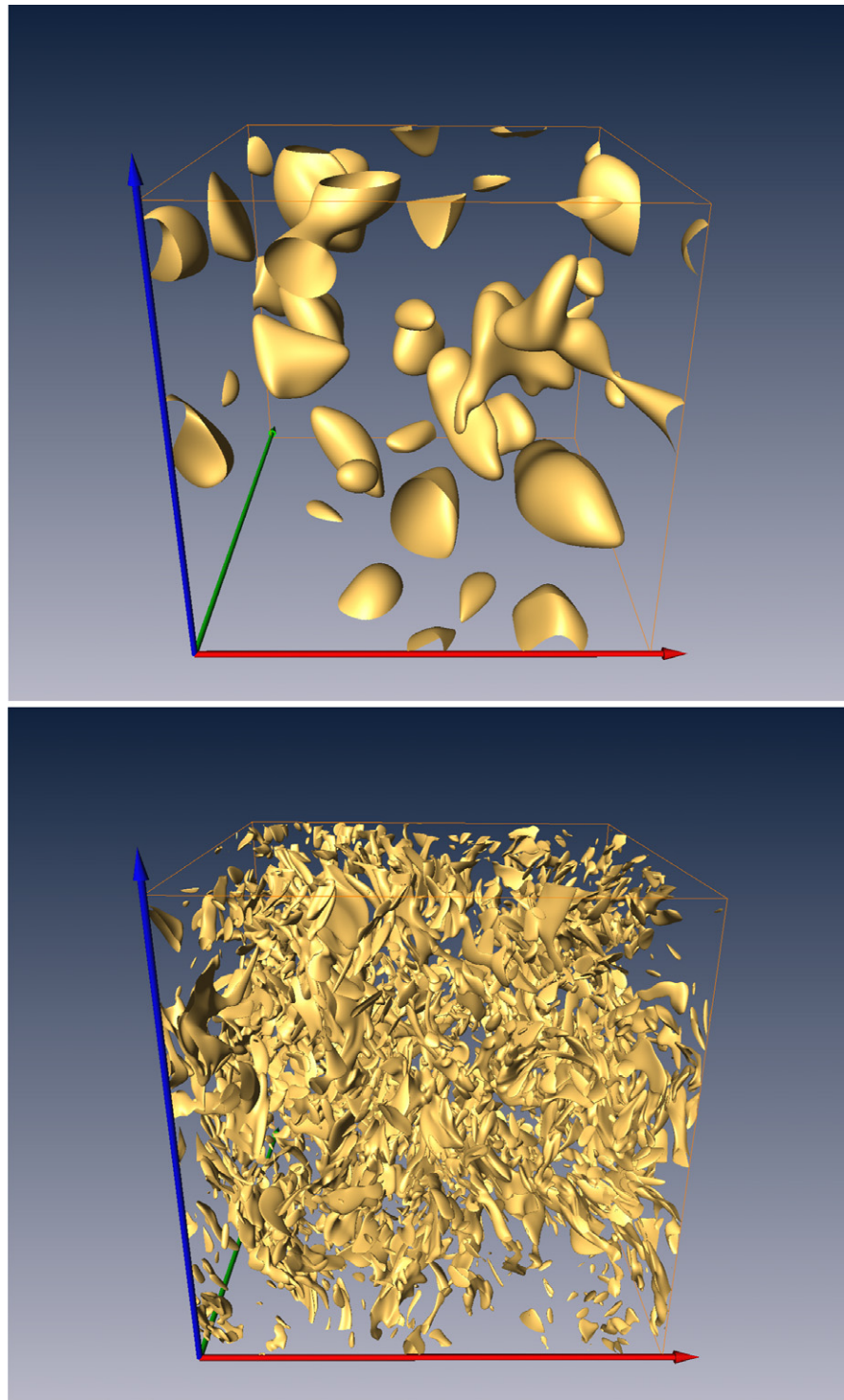
Figure 8. Morphological manifestation of the crossover from Gaussian to non-Gaussian velocity gradient statistics. Isolevel plots of snapshots of $|\partial u/\partial x|$ for run 1 at $R_\lambda = 10$ (top) and for run 4 at $R_\lambda = 65$ (bottom) are shown. Both level sets were taken at the corresponding values of $2 \times (\partial u/\partial x)_{\mathrm{rms}}$. We observe a significant increase of the spatial intermittency for the higher Reynolds number data set.

Our work suggests that the scaling exponents of the moments of velocity derivatives observed in the relatively low-Reynolds-number turbulent flow, lacking even traces of the inertial range, can be expressed in terms of the inertial-range exponents corresponding to the *asymptotic* case ($Re \to \infty$). We stress that the scaling exponents ρ_n and d_n of the moments of velocity derivatives and dissipation rate reach asymptotic values that are independent of large-scale Reynolds number, even at low values of the Reynolds numbers. Thus, the dynamics of velocity fluctuations at the scales $r \approx \eta$ are asymptotic even in relatively low-Reynolds-number flows. This could mean that the magnitudes of inertial-range exponents ($Re \to \infty$) are prescribed by the matching conditions on the ultra-violet cut-offs formed in the low-Reynolds-number regimes. The relation of the observed behaviour to fluctuations of the dissipation scale will be discussed elsewhere.

Acknowledgments

References

[1] Kolmogorov A N 1941 The local structure of turbulence in incompressible viscous fluid for very large Reynolds number *Dokl. Akad. Nauk SSSR* **30** 9–13

[2] Anselmet F, Gagne Y and Hopfinger E J 1984 High-order velocity structure functions in turbulent shear flows *J. Fluid Mech.* **140** 63–89

[3] Kolmogorov A N 1962 A refinement of previous hypotheses concerning the local structure of turbulence in a viscous incompressible fluid at high Reynolds number *J. Fluid Mech.* **13** 82–5

[4] Oboukhov A M 1962 Some specific features of atmospheric turbulence *J. Fluid Mech.* **13** 77–81

[5] Sreenivasan K R and Antonia R A 1997 The phenomenology of small-scale turbulence *Annu. Rev. Fluid Mech.* **29** 435–72

[6] Frisch U 1995 *Turbulence—The Legacy of A N Kolmogorov* (Cambridge: Cambridge University Press)

[7] Sreenivasan K R and Meneveau C 1988 Singularities of the equations of fluid motion *Phys. Rev.* A **38** 6287–95

[8] Paladin G and Vulpiani A 1987 Degrees of freedom of turbulence *Phys. Rev.* A **35** 1971–3

[9] Nelkin M 1990 Multifractal scaling of velocity derivatives in turbulence *Phys. Rev.* A **42** 7226–9

[10] Frisch U and Vergassola M 1991 A prediction of the multifractal model—the intermediate dissipation range *Europhys. Lett.* **14** 439–44

[11] Chevillard L, Castaing B and Lévêque E 2005 On the rapid increase of intermittency in the near-dissipation range of fully developed turbulence *Eur. Phys. J.* B **45** 561–7

[12] Bowman J C, Doering C R, Eckhardt B, Davoudi J, Roberts M and Schumacher J 2006 Links between dissipation, intermittency, and helicity in the GOY model revisited *Physica* D **218** 1–10

[13] Yakhot V 2001 Mean-field approximation and a small parameter in turbulence *Phys. Rev.* E **63** 026307

[14] Yakhot V and Sreenivasan K R 2004 Towards a dynamical theory of multifractals in turbulence *Physica* A **343** 147–55

IOP Institute of Physics ⚛ DEUTSCHE PHYSIKALISCHE GESELLSCHAFT

[15] Yakhot V 2006 Probability densities in strong turbulence *Physica* D **215** 166–74
[16] Eggers J and Grossmann S 1991 Does deterministic chaos imply intermittency in fully developed turbulence *Phys. Fluids* A **3** 1958–68
[17] Schumacher J 2004 Relation between shear parameter and Reynolds number in statistically stationary turbulent shear flows *Phys. Fluids* **16** 3094–102
[18] Pope S B 2000 *Turbulent Flows* (Cambridge: Cambridge University Press)
[19] Chen S Y, Doolen G, Herring J R, Kraichnan R H, Orszag S A and She Z S 1993 Far-dissipation range of turbulence *Phys. Rev. Lett.* **70** 3051–4
[20] Hill R J 2001 Equations relating structure functions of all orders *J. Fluid Mech.* **434** 379–88
[21] Kurien S and Sreenivasan K R 2001 Dynamical equations for higher-order structure functions, and a comparison of a mean-field theory with experiments of three-dimensional turbulence *Phys. Rev.* E **64** 056302
[22] Gotoh T and Nakano T 2003 Role of pressure in turbulence *J. Stat. Phys.* **113** 855–74
[23] She Z S and Lévêque E 1994 Universal scaling laws in fully developed turbulence *Phys. Rev. Lett.* **72** 336–9
[24] Chen S Y, Dhruva B, Kurien S, Sreenivasan K R and Taylor M A 2005 Anomalous scaling of low-order structure functions of turbulent velocity *J. Fluid Mech.* **533** 183–92
[25] Kolmogorov A N 1941 Dissipation of energy in locally isotropic turbulence *Dokl. Akad. Nauk SSSR* **32** 19–21
[26] Falkovich G and Sreenivasan K R 2006 Lessons from hydrodynamic turbulence *Phys. Today* **59** 43–9
[27] Benzi R, Ciliberto S, Tripiccione R, Baudet C, Massaioli F and Succi S 1993 Extended self-similarity in turbulent flows *Phys. Rev.* E **48** R29–R32